Atmospheric Entry Studies for Venus Missions: 45° Sphere-Cone Rigid Aeroshells and Ballistic Entries

Dinesh K. Prabhu
ERC, Inc./NASA Ames Res. Center
Mail Stop 229-1
Moffett Field, CA 94035
(650) 604-1145
Dinesh.K.Prabhu@nasa.gov

Gary A. Allen, Jr.
ERC, Inc./NASA Ames Res. Center
Mail Stop 230-2
Moffett Field, CA 94035
(650) 604-4228
Gary.A.Allen@nasa.gov

Gelsomina Cappuccio
NASA Ames Res. Center
Mail Stop 229-3
Moffett Field, CA 94035
(650) 604-1313
Mina.Cappuccio@nasa.gov

Thomas R. Spilker
Solar System Science & Exploration
457 Granite Avenue
Monrovia, CA 91016

planetaryflightarchitect@yahoo.com

Helen H. Hwang
NASA Ames Res. Center
Mail Stop 230-3
Moffett Field, CA 94035
(650) 604-1368
Helen.Hwang@nasa.gov

Robert W. Moses
NASA Langley Res. Center
Mail Stop 489
Hampton, VA 23681
(757) 864-8675
Robert.W.Moses@nasa.gov

***Abstract*—The present study considers direct ballistic entries into the atmosphere of Venus using a 45° sphere-cone rigid aeroshell, a legacy shape that has been used successfully in the past in the Pioneer Venus Multiprobe Mission. For a number of entry mass and heatshield diameter combinations (*i.e.*, various ballistic coefficients) and entry velocities, the trajectory space in terms of entry flight path angles between skip out and –30° is explored with a 3DoF trajectory code, *TRAJ*. From these trajectories, the viable entry flight path angle space is determined through the use of mechanical and thermal performance limits on the thermal protection material and science payload; the thermal protection material of choice is *entry-grade* carbon phenolic, for which a material thermal response model is available. For mechanical performance, a 200 g limit is placed on the peak deceleration load experienced by the science instruments, and 10 bar is assumed as the pressure limit for *entry-grade* carbon-phenolic material. For thermal performance, inflection points in the total heat load distribution are used as cut off criteria. Analysis of the results shows the existence of a range of "critical" ballistic coefficients beyond which the steepest possible entries are determined by the pressure limit of the material rather than the deceleration load limit.**

TABLE OF CONTENTS

1. INTRODUCTION

In its latest survey, titled "Visions and Voyages for Planetary Science in the Decade 2013-2022," [1] the National Research Council (NRC) has recommended several *Flagship* or *New Frontiers* class robotic missions to various planetary destinations including Earth. The missions to Venus and Saturn recommended in the Decadal Survey, which have an atmospheric entry component in their mission profiles, are based on the results of several concept studies [2-6].

To further understand the *entry* technology needs of *Flagship* and *New Frontiers* class missions to Venus and Saturn recommended in the NRC Decadal Survey, NASA's In-Space Propulsion Technology (ISPT) program sponsored a rapid study with a team drawn primarily from Ames and Langley Research Centers (ARC and LaRC). The objectives of the study team were: (i) to analyze which entry technologies would be appropriate, (ii) to identify and/or quantify gaps/shortfalls in these technologies, and (iii) to explore whether any of the new technologies in which the Space Technology Program (STP) of NASA has been investing, could possibly enlarge entry trade space for these missions.

To meet the stated objectives, the study team performed a survey of past missions (actual or proposed) [2-9] to Venus and the Outer Planets. Based on the information gathered for Venus missions, the team then examined/analyzed three entry scenarios for a rigid aeroshell atmospheric entry probe: (i) direct entry *vs*. entry from orbit, (ii) ballistic *vs*. lifting entry (including aerocapture), and (iii) low L/D *vs*. mid-L/D entry with alternate shapes. The team did not explore scenarios with new/emerging entry technologies, which are still in early development. As such, the study team decided that the short time available was best expended in establishing performance baselines for "traditional" entry configurations, *i.e.*, rigid aeroshell configurations with well-characterized thermal protection materials, so that future comparisons with emerging technologies could be made.

The three new Venus mission concepts (*Flagship* or *New Frontiers* class) that provided inputs to the NRC Decadal

Survey are: (i) *V*enus *M*obile *E*xplorer (VME) [2], (ii) *V*enus *I*ntrepid *T*essera *L*ander (VITaL) [3], and (iii) *V*enus *C*limate *M*ission (VCM) [4]. All three concept missions, like the Pioneer Venus mission, are predicated upon a 45° sphere-cone rigid aeroshell geometry for the entry probe/system. Some salient points of these concept designs are:

(i) Maximum entry masses range from 850 kg (VCM) to 3000 kg (VITaL and VME).
(ii) Heatshield diameters range from 2.0 m (VCM) to 3.5 m (VITaL and VME).
(iii) Estimated peak deceleration loads are under 200 g's, while entry flight path angles range from −19° (VCM and VME) and −23.4° (VITaL).
(iv) The heatshields are made of high-density carbon phenolic (combination of tape-wrapped and chop-molded varieties).
(v) The backshells have a tiled thermal protection system using PICA (Phenolic Impregnated Carbon Ablator).

Of particular interest to the present study is VITaL, which has both *in situ* atmospheric measurements *and* surface science in its mission objectives. Since VITaL's mission profile includes a lander, the entry probe is significantly larger (3.5 m dia.) and heavier (2100 kg) than the largest probe (1.4 m dia. and 316 kg) of the Pioneer Venus Multiprobe mission. Furthermore, VITaL also includes sensitive instruments, *e.g.*, the Raman/Laser-Induced Breakdown Spectroscopy or Raman/LIBS experiment, the apparatus for which has not been qualified for deceleration loads of the order of hundreds of Earth g's (quite typical of ballistic entries into Venus). Keeping deceleration loads under a 200 g limit, so that flight qualification of the scientific apparatus is not too expensive, is a key trade in the design of the entry system for Venus.

Definitions

The entry ballistic coefficient, or simply EBC, is defined as:

$$\beta_E = \frac{m_E}{C_D A_b} \qquad A_b = \tfrac{1}{4}\pi D_b^2 \tag{1}$$

where m_E, D_b, and A_b are respectively the mass, base diameter, and base area of the heatshield. The hypersonic drag coefficient, C_D, is usually estimated from Newtonian impact theory and is nearly constant in the hypersonic phase of entry. However, the drag coefficient does depend on the geometry of the heatshield, *e.g.*, C_D for a 45° sphere-cone is 1.05, while it is 1.7 for a 70° sphere-cone. Using Eq. 1, the EBCs of PVLP and VITaL are 190 kg/m^2 and 208 kg/m^2, respectively.

The entry flight path angle, or simply EFPA, is the angle the capsule's velocity vector makes with the local horizon at entry interface.

In an earlier survey of Venus entries, Venkatapathy *et al.* [10] systematically explored the entry ballistic coefficient (β_E) and entry flight path angle (γ_E) space for 45° sphere-cone heatshields derived from the Pioneer Venus Large Probe (PVLP).

A key result from the survey of Venkatapathy *et al.* [10] is reproduced here as Fig. 1, which shows the contour level curves of peak stagnation point total heat flux (in W/cm^2), total heat load (in J/cm^2), and peak deceleration loads (in Earth g's) for an entry velocity (V_E) of 11.5 km/s.

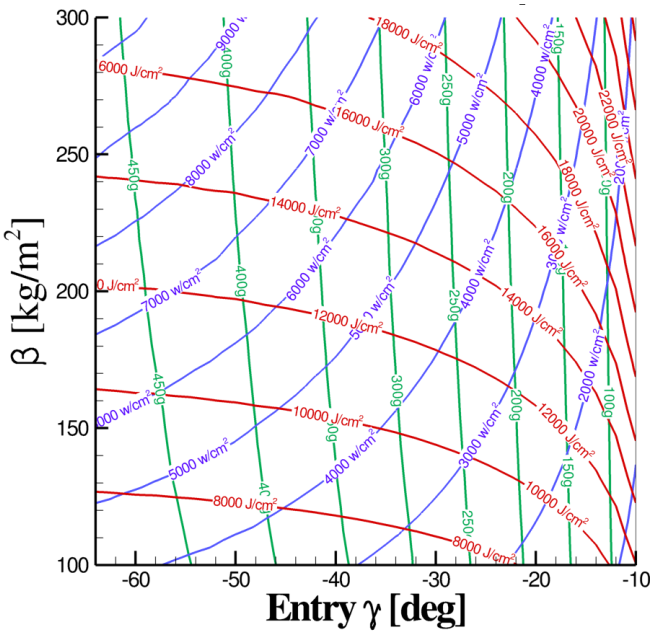

Figure 1 (reproduced from Ref. 10). Contours of peak total (convective and radiative) heat flux (blue lines), total heat load (red lines), and peak deceleration load (green lines) for PVLP-derived vehicles over a range of entry flight path angles. Contours are for an entry velocity of 11.5 km/s.

From Fig. 1 it is clear that to keep the deceleration loads under 200 Earth g's, it is necessary to constrain entry flight path angles (EFPAs) to an interval between −25° and skip out for entry ballistic coefficients up to 300 kg/m^2.

The survey conducted by Venkatapathy *et al.* [10] did not consider the thermal protection material for the heatshield, and left that choice to be made based on the estimated peak heat flux, as is the standard practice in early entry system analysis. In contrast to the approach taken in the aforementioned survey, the present study explores the entry trajectory space for a *prescribed* thermal protection material.

The material chosen here for the heatshield is high-density *entry-grade carbon phenolic*. Within the context of NASA, the term "high-density entry-grade carbon phenolic," or simply entry-grade carbon phenolic, refers to a material manufactured to precise specification involving precursor rayon material, carbonization, and processing. Further details of carbon phenolic are outside the scope of this study and are available elsewhere [11].

There are two varieties of this entry-grade carbon phenolic – chop molded and tape wrapped – with the chop molded variety being unique to NASA missions using the 45° sphere-cone rigid aeroshell; the chop-molded variety is used on the spherical nose cap. We note here that although there are other commercially available carbon phenolics, such as PICA (used in the Stardust and MSL/Mars Science Laboratory missions, for example) and nozzle liner-grade carbon phenolic (used in the Space Shuttle SRBs/Solid Rocket Boosters, for example), these materials are not considered and are beyond the scope of the present study.

Entry-grade carbon phenolic is a robust and flight-proven thermal protection material that is capable of withstanding the severe aerothermal environments (pressures of 8-17 bars, shear stresses of the order of 2-10 kPa, and heat fluxes of the order 4-10 kW/cm^2) associated with ballistic entries into Venus. It has been used successfully in the Pioneer Venus Multiprobe and Galileo missions, and in the Hayabusa mission as well. Furthermore, the performance of this material has been very well characterized through both ground tests and flight (for both defense and civil applications), and a calibrated thermal response model is available [12] for it in *FIAT* [13], a NASA-developed one-dimensional material response code.

The present study is a more focused examination of entry parameters (velocity, ballistic coefficient and flight path angle) *and* environments (deceleration loads, pressures, heat fluxes, *etc.*) relevant to the new Venus *Flagship* and *New Frontiers* missions. This detailed examination, in turn, facilitates identification of technology gaps/shortfalls (if any) in the mission design trade space for the legacy architecture, *i.e.*, a 45° sphere-cone rigid aeroshell with a known thermal protection material. Furthermore, EFPA baselines derived for the legacy architecture allow for comparison with results from analyses for other rigid aeroshell entry scenarios, such as lifting entries of different probe geometries (70° sphere-cone, ellipsleds, or even asymmetric shapes) and with alternate thermal protection material. Such baselines could also be used to define performance requirements for new deployable architectures, and/or new thermal protection materials.

The primary objectives of the present study are: *(i) to develop the entry trajectory space – parameterized by V_E, β_E, and γ_E – for direct ballistic entries into Venus with a 45° sphere-cone rigid aeroshell geometry and entry-grade carbon phenolic as the choice of heatshield material, and (ii) to determine the range of γ_E, for various V_E and β_E combinations, for which missions to Venus are viable using a legacy entry system architecture*. We do not consider lifting entries in the present study. Details of such a study, performed by another group within the larger team, will be available in a forthcoming publication [14].

Having established the general context for exploration of an entry trajectory space, we describe the methodology next. We emphasize here that 3DoF flight trajectories are independent of the choice of thermal protection material, *i.e.*, the predicted deceleration loads, pressures, heat fluxes, and heat loads, *do not* depend on the choice of material. The standard procedure is to develop flight trajectories (with dispersions perhaps) and select the thermal protection material that is appropriate to the margined predicted peak heat flux. The selected material is then sized to the margined total heat load for the worst-case trajectory. In the present study, we have already made the choice of material – entry-grade carbon phenolic – regardless of what deceleration loads, or pressures, or heat fluxes are predicted by *TRAJ*. It is on the databank of unconstrained trajectories developed here that we impose performance constraints to determine the viable entry trajectory space.

2. METHODOLOGY

The present paper makes no attempt to "design" a thermal protection system. It merely attempts to establish the viable entry trajectory space for a rigid aeroshell to which entry-grade carbon phenolic (the basis for several *New Frontiers* or *Flagship* class Venus mission concepts) is bonded. The following ground rules, assumptions, and processes have been used for the trajectory analyses to be presented here:

1. The heatshield configuration is a 45° sphere-cone for which the hypersonic drag coefficient is 1.05. The geometry and the four parameters – R_b, R_n, R_s, and θ_c – that completely describe it are shown in Fig. 2. The nose and shoulder radii are often expressed as fractions – R_n/R_b and R_s/R_b – of the base radius. For all cases in the present study $R_n/R_b = 0.5$, and $R_s/R_b = 0$.

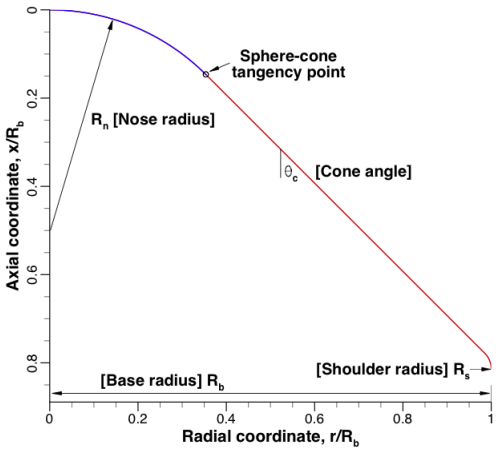

Figure 2. Geometry of a sphere-cone heatshield. The axisymmetric geometry is described by four parameters – (i) base radius, R_b, (ii) spherical nose radius, R_n, (iii) a toroidal shoulder radius, R_s, and (iv) the cone half angle, θ_c.

2. The entry interface altitude at Venus is taken as 200 km.
3. The VIRA/VenusGRAM model [15] is used for the atmosphere.
4. 3DoF flight trajectories are constructed using NASA ARC's in-house 3DoF code, *TRAJ* [16]. The input variables used by *TRAJ* are: m_E (entry mass), R_b (base

radius), C_D (drag coefficient—computed using Newtonian impact theory, if an experimental/flight drag database is not readily available), R_n (nose radius), R_s (shoulder radius), V_E (inertial entry velocity), ψ_E (inertial heading angle), γ_E (inertial EFPA), and ϕ_E (longitude).

5. The 3DoF simulations are terminated when the Mach number reaches a value of 0.8 along the trajectory. It is assumed that the heatshield is jettisoned and a parachute deployed at Mach 0.8.
6. Aerothermal environments at the *stagnation point* are estimated along a flight trajectory through correlations that depend only on the freestream density (ρ_∞) and flight velocity (V_∞), and the nose radius (R_n) of the heatshield. We have the following correlations:

$$\begin{aligned} p_{\text{stag}} &\approx \rho_\infty V_\infty^2 \\ q_{\text{stag,conv.}} &= C_{\text{conv}} \frac{\sqrt{\rho_\infty} V_\infty^{3.04}}{\sqrt{R_n}} \\ q_{\text{stag,rad.}} &= C_{\text{rad}} \sqrt{R_n} \rho_\infty^{1.2} V_\infty^b \end{aligned} \tag{2}$$

   where C_{conv}, C_{rad} and b are constants. The stagnation point convective heat flux correlation is a variant of the Fay-Riddell correlation [17], and the stagnation point radiative heat flux correlation is due to Tauber [18]. No margins, to account for either atmospheric uncertainties or uncertainties in aerothermal environments (pressure, shear stress, and heat flux), are applied to the estimated stagnation point values. Note: shear stress is not considered in the present study – its value is zero at the stagnation point, by definition. However, shear levels, especially turbulent shear levels, can be large on the conical frustum.
7. Peak values of radiative, convective, and total heating at the stagnation point, the peak pressure at the stagnation point, the peak deceleration loads, and total heat load (integrated heat flux over the time of flight) are recorded for each trajectory simulated.
8. The heatshield material is sized using the *FIAT* [13] option integrated into *TRAJ*. It requires specification of the material stack, initial temperature, and a bondline temperature constraint. The material stack used in the present study consists of 3 layers – (i) an outer layer of entry-grade carbon phenolic (the thickness of this layer is determined by *FIAT*), (ii) an intermediate layer of RTV-560 (adhesive), and (iii) an inner layer of aluminum (the carrier structure). The initial temperature of the stack is set to 18 °C [19]. This material stack is similar to that described in the the Pioneer Venus Large and Small Probe Data Book [20] and the report of Talley [21].
9. *FIAT*, a materials thermal response code, has a model for entry-grade carbon phenolic [12]. Note: The present work does not make any distinction between the chop-molded and tape-wrapped varieties of entry-grade carbon phenolic, insofar as their material thermal properties are concerned. The thermal response of carbon phenolic is computed for the total heat load estimated from the 3DoF simulation and with the specified stack. The material is sized to a bondline limit temperature of 250 °C (a safe limit of RTV-560 adhesive [22]). Sizing is performed for the stagnation point only.
10. Assuming uniform thickness, the mass of the thermal protection system (TPS) or heatshield is determined using the computed thickness (t_{CP}) as:

$$m_{\text{CP}} = \rho_{\text{CP}} A_{\text{wet}} t_{\text{CP}} \tag{3}$$

    where ρ_{CP} is the mass density of carbon phenolic and A_{wet} is the wetted area of the heatshield. No margins, to account for uncertainties in material properties, are applied to the computed thickness (often referred to as the zero-margin thickness).
11. This *TRAJ-FIAT* process (Steps 4 through 10) is then repeated for multiple values of γ_E in the interval of interest (from skip out to -30°). Note: there are no margins on the entry flight path angles. Such margins are necessary to account for atmospheric uncertainties and interplanetary trajectory delivery errors [23].
12. Once a databank has been created for (i) trajectories, (ii) environments along those trajectories, and (iii) heatshield mass estimates for those environments, we impose constraints *a posteriori* to determine the EFPA window for a given entry mass and vehicle size for which atmospheric entry is feasible.

We consider temporal variations of aerothermal environments at one spatial location on the heatshield, *viz*. the stagnation point. Strictly speaking, spatial distributions of aerothermal environments are also needed since there could be trajectory time periods where environments away from the stagnation point could be higher. For instance, for a 45° sphere-cone we expect flow transition to turbulence, with consequent heating augmentation on the conical flank. There are no built-in correlations currently in *TRAJ* [16] to estimate this augmented heat flux, and the only way to do so is to compute flow field solutions using numerical simulation tools – *DPLR* [24] for convective heating and *NEQAIR* [25] for radiative heating, for example. Such an undertaking at this level of analysis was deemed unnecessary, especially since literally thousands of flight trajectories were generated for V_E-β_E-γ_E combinations.

Since the present work is focused on the stagnation point alone, we have opted to assume a uniform thickness for the heatshield. This assumption also appears to be consistent with the mission concept studies presented in Refs. 2-4. We note that the Pioneer Venus probes did not have uniformly thick heatshields – the thickness of the spherical nose cap (chop-molded carbon phenolic) was greater than that over the conical flank (tape-wrapped carbon phenolic) [21]. Complicating matters further, the facesheet thicknesses in the two regions were also different [21].

Finally, the present study does not consider the backshell in the analysis, since the mass of the thermal protection system (TPS) of the backshell is usually a small fraction (< 10%) of

the heatshield mass. For example, the mass of the thermal protection system for the heatshield of PVLP was 27.3 kg and that for the backshell was 1.51 kg (roughly 6% of the total mass of the TPS) [20,21].

The strategy adopted in the present work is to first anchor the methodology to Pioneer Venus – the sole source of openly available engineering data. Replication of unmargined thickness (at the stagnation points of the Large Probe and the Day Probe) is then taken to be a measure of success of our process.

3. Entry Trajectory Space & Case Matrix

As mentioned earlier, our development of atmospheric entry trajectories explores a space parameterized by: (i) the inertial entry velocity, V_E, (ii) the entry ballistic coefficient, β_E, and (iii) the inertial entry flight path angle, γ_E. The ranges of values for these parameters in the present study are guided by the mission concept studies [2-4] performed for the Decadal Survey.

Entry velocity

We assume that the inertial entry velocity (or a range of velocities), V_E, is provided by the interplanetary trajectories developed using a combination of launch/arrival dates and launch system. In the present study we consider three representative entry velocities – 10.8, 11.2, and 11.6 km/s. A velocity of 11.6 km/s is consistent with PVLP (11.54 km/s), and 11.2 km/s is consistent with the mission concept studies [2-4].

Entry ballistic coefficient (EBC)

We have chosen to sample a small number of ballistic coefficients between 100 kg/m^2 and 400 kg/m^2, which are respectively 0.5× and 2× that of PVLP.

We separate out the mass and heatshield size in the definition of ballistic coefficient and consider 24 combinations—8 entry masses between 1500 kg to 2750 kg, and 3 heatshield diameters of 2.5, 3.5, and 4.5 m.

The entry mass and heatshield diameter combination, along with C_D (=1.05) of the 45° sphere-cone, help fix the EBC (Eq. 1). The EBCs for the various m_E-D_b combinations we have chosen are shown in Table 1.

The 3.5 m-2000 kg combination has an EBC of 198 kg/m^2, which is close to that of VITaL (208 kg/m^2) and PVLP (190 kg/m^2).

We note here that some of the m_E-D_b combinations might not be physically realizable, either because packing becomes an issue or because the heatshield mass becomes excessive. It is the latter issue that the present paper deals with.

Table 1. Entry ballistic coefficients for various heatshield configurations considered for Venus entry

	Diameter, m		
	2.5	**3.5**	**4.5**
Mass, kg	**Ballistic coefficient, kg/m^2**		
1500	291	148	90
1750	340	173	105
2000	388	198	120
2250	437	223	135
2750	534	272	165

.

Entry flight path angle (EFPA)

Depending on the entry velocity and ballistic coefficient, there is a limiting shallow entry angle beyond which the capsule will skip out of the atmosphere. Therefore, the present study samples the entry angle variable at values more negative than the skip out angle, *i.e.*, for entries that are *steeper* than skip out [23]. Further, to keep the deceleration loads below 250 g (Fig. 1), the steepest EFPA is −30°. Therefore, the EFPA interval considered in the present study is between skip out and −30°. This interval is divided into 0.5° sub-intervals for 3DoF trajectory computations.

For each entry velocity and EBC combination, the *TRAJ-FIAT* combination (Step 12 of the methodology outlined) is used to develop flight trajectories for the range of entry angles chosen and for each trajectory entry-grade carbon phenolic is sized (without any margins) to the computed heat load at the stagnation point. We then determine viable entry flight path angle windows through *a posteriori* application of constraints.

4. Constraints

We categorize constraints into two types— mechanical, and thermal. The former category includes deceleration loads and pressures, while the latter includes heat fluxes and heatshield mass estimates. *Although the categorization is simple and straightforward, there is subjectivity in the choice of limiting values of some of these constraints.*

Mechanical constraints

The mechanical performance constraints determine how steeply an entry can be without violating either the specified deceleration load limit or the stagnation point pressure limit.

Peak deceleration load limit: Peak deceleration load is a mission specification, and is relevant to the science payload, *not* the thermal protection material. It is a critical performance parameter because it drives the qualification/flight certification of science instruments. The mission profiles of the concept studies [2-4] performed for the Decadal Survey have peak deceleration loads between 150 to 200 g. It should be borne in mind that the deceleration load limit is only on each science instrument and *not* on the entire entry system. Presumably centrifuges

that can test up to these loads are available. Therefore, *we set the upper limit on deceleration load to 200 g*.

Stagnation point pressure limit: If we knew the pressure at which the char (due to ablation) of entry-grade carbon phenolic fails mechanically (or spalls), then that pressure value could be imposed as a constraint. Unfortunately, however, this limit is not readily available in the open literature, nor is there any NASA arc-jet test experience to specify such a value. Therefore, the limit we have chosen here is a subjective one, and is based on flight experience in the Pioneer Venus and Galileo Jupiter missions. PVLP experienced pressures slightly higher than 10 bars, as did the Galileo probe to Jupiter [26]. However, we know that the Night and North probes of Pioneer Venus experienced pressures greater than 10 bars and survived the entry [27]. Erring on the side of caution, *we impose a pressure limit of 10 bars for entry-grade carbon phenolic*.

One question to ask here is whether constraints on peak deceleration loads *and* peak loads can be active simultaneously, or would the choice of one preclude the other? We make an attempt to answer this question in the Results section.

Thermal Performance Constraint

The thermal performance constraint, which is primarily the total heat load (equivalently the estimated total mass of the entry-grade carbon phenolic heatshield), determines how shallow the EFPA can be. Strictly speaking, the EFPA corresponding to skip out represents the closure of the EFPA window at the shallow end. However, the high heat loads at shallow EFPAs might result in prohibitively high heatshield masses because of the lack of insulative capability in entry-grade carbon phenolic.

Total heat load limit: Since for each V_E-β_E combination, we have estimates of total heat load (Q) as a function of EFPA (γ_E), we can determine the "knee in the curve," *i.e.*, determine the EFPA at which the curvature, $\kappa(\gamma_E)$,

$$\kappa(\gamma_E) = \pm \frac{\frac{d^2Q}{d\gamma_E^2}}{\left[1+\left(\frac{dQ}{d\gamma_E}\right)^2\right]^{\frac{3}{2}}} \tag{4}$$

of the $Q(\gamma_E)$ distribution attains an extremum. A few things to note in working with this criterion: (i) the total heat load is independent of the choice of material, and (ii) the distribution of Q with γ_E is discrete and application of Eq. 4 requires evaluation of first and second derivatives. Since numerical differentiation can be "noisy," we fit the discrete distributions with smooth curves and evaluate the extrema analytically. This is discussed later in the Results section.

Mass fraction limit: The mass fraction of the heatshield is defined as:

$$f_{CP} = \frac{m_{CP}}{m_E} \tag{5}$$

where m_{CP} is the mass of the heatshield assuming a uniform thickness, and the thickness estimate is provided by application of *FIAT* to *TRAJ*-predicted total heat loads.

The choice of a value for mass fraction limit is largely a subjective one, and depends on the mission. The only two openly available data points from Venus missions are from the Large and Day probes of Pioneer Venus. The Night and North probes of Pioneer Venus are not relevant because their entries were considerably steeper than the -30° limit we have imposed in the present study. For the Large Probe (γ_E = –32.5°), the mass fraction of the as-flown heatshield was only 0.09, while it was 0.13 for the Day Probe (γ_E = –25.4°). The differing mass fractions for the Large and Day probes of Pioneer Venus suggest a dependence on EFPA. However, the North and Night Probes, which were identical to the Day Probe, had the *same* mass fraction despite significant differences in their entry flight path angles.

The mass fraction estimates provided by the concept studies [2-4] are greater than 0.13 – the reports provide an estimate of the thickness of the heatshield material, which can be converted to a mass equivalent using Eq. 2.

In the present work, we leave open the choice of mass fraction, preferring instead to examine instead the effects of making various choices. Furthermore, we assume that this mass fraction value is a constant across the entire viable EFPA space.

5. RESULTS & DISCUSSION

Process Verification

We first verify our procedure outlined in the Methodology section. Two good candidates for verification are: (i) PVLP (316.5 kg, 1.42 m dia., 45° sphere-cone), which had an EBC of 190 kg/m^2, an entry velocity of 11.54 km/s, and an EFPA of –32.4° [26], and (ii) Pioneer Venus Day Probe (91 kg, 0.76 m dia., 45° sphere-cone), which had an EBC of 190 kg/m^2, an entry velocity of 11.54 km/s, and an EFPA of –25.4° [26].

Applying our procedure to these two cases yielded the following results:

1. PVLP: The simulated thickness (for the material stack shown in Table 1) was 0.79 cm, while the *unmargined* thickness reported in Ref. 20 was 0.762 cm at the stagnation point.
2. Day Probe: The simulated thickness (for the material stack shown in Table 1) was 0.87 cm, while the *unmargined* thickness reported in Ref. 20 was 0.864 cm.

The agreement between results of the current methodology and the unmargined thicknesses of the Pioneer Venus

program is fortuitous, given the differences in materials of the carrier structure and the adhesives [20,21]. Nevertheless, the results give us confidence in sizing at the stagnation point.

Having anchored the methodology against PVLP, we present results for the nominal cases, *i.e.*, a 2000 kg entry mass for three entry velocities – 10.8, 11.2, and 11.6 km/s – and EFPAs ranging from skip out to -30°.

Nominal Cases: Mechanical constraint (peak deceleration load)

Figure 3 shows the variation with EFPA of peak deceleration loads for an entry mass of 2000 kg. Curves are shown for all three entry velocities and three EBCs – 120, 198, and 388 kg/m^2 (a factor of 3 spread between low and high). We observe the following:

(i) Peak deceleration loads increase with increasing EFPA for *all* entry velocities and ballistic coefficients, which is as expected.
(ii) For a given EBC (curves of one family—solid, or dashed, or dash-dotted) the highest deceleration loads correspond to the highest entry velocity (11.6 km/s). Between the highest and lowest entry velocities, the deceleration loads at an EFPA of –30° differ by no more than 15%.
(iii) For a given entry velocity (curves of one color – red, or green, or blue) the highest deceleration loads correspond to the *lowest* ballistic coefficient (120 kg/m^2). Between the highest and lowest ballistic coefficients, the maximum difference in deceleration loads at an EFPA of –30° is less than 12%.
(iv) The small box (0.5° × 10 g) shown in Fig. 3 represents the region where the peak deceleration load is nearly independent of entry velocity *and* ballistic coefficient.

Since the highest deceleration loads occur for the highest entry velocity of 11.6 km/s for all three ballistic coefficients, it is sufficient to work with curves corresponding to this entry velocity to determine the steepest entry angles for a prescribed deceleration load limit.

Dashed horizontal lines at 100 and 200 g are also shown in Fig. 3. The intersections of these lines with the peak deceleration curves for the highest entry velocity (11.6 km/s) are shown as dashed vertical lines in the plot. The arrows indicate the direction in which the vertical lines move with decreasing deceleration load limits to suggest that the deceleration load limit determines the steepest entry flight path angle.

If the deceleration load limit is 200 g, then the steepest EFPA is roughly -23.5° for an EBC of 388 kg/m^2, and –21.5° for an EBC of 120 kg/m^2, which is only a 2° interval for a factor of 3 difference in ballistic coefficients. If deceleration loads cannot exceed 100 g (because either instruments cannot be qualified beyond this value or it becomes exceedingly expensive to qualify instruments beyond this value), then the steepest EFPA is –13.25° for a ballistic coefficient of 388 kg/m^2, and -12.5° for an EBC of 120 kg/m^2, which is now only a 0.75° interval. Therefore, as the deceleration load limit is decreased, the ballistic coefficient becomes less relevant, while at a 50 g limit, the steepest EFPA is only about –9.5° for *all* ballistic coefficients.

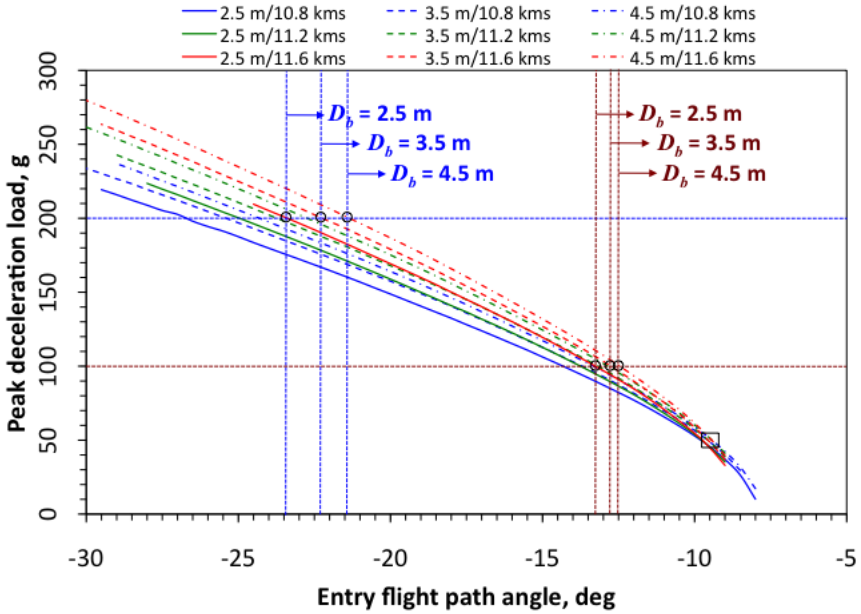

Figure 3. Variation with EFPA of peak deceleration load for m_E= 2000 kg and various entry velocities. Horizontal dashed lines are shown at 100 and 200 g, and at the intersections of these lines with the peak deceleration load curves, the corresponding EFPAs are shown as vertical dashed lines. At roughly 50 g the deceleration load is nearly independent of entry velocity *and* ballistic coefficient.

Instead of the cumbersome graphical approach (Fig. 3), we can use an alternative analytical approach. In the analytical approach, we fit to the peak deceleration loads curves of the form

$$g_{Peak}(\gamma_E) = A(V_E,\beta_E)\left[\Gamma(V_E,\beta_E) - \gamma_E\right]^{\phi(V_E,\beta_E)} \qquad (6)$$

where A, Γ, and ϕ are curve-fit coefficients that (could) depend on both entry velocity and EBC. The coefficient Γ can be interpreted as the skip out angle. For a prescribed value of g_{Peak}, Eq. 6 is easily inverted to obtain the corresponding value of EFPA, γ_E. This provides a cross check against results of the graphical method.

Figure 4 shows a sample fit to peak deceleration loads for a 3.5 m diameter heatshield of 2000 kg entry mass and an entry velocity of 11.6 km/s. The values of A, Γ, and ϕ obtained by fitting the data are also shown in the figure.

Applying Eq. 6 to all peak deceleration load curves (all nine of them) shown in Fig. 3 results in the entries shown in Table 2. The inflections in Γ and ϕ at 11.2 km/s are interesting, but cannot be explained easily without finer resolution in entry velocity. The dependence of the curve-fit coefficients on either entry velocity or EBC could be pursued further. However, such an undertaking will require much finer resolution in both variables.

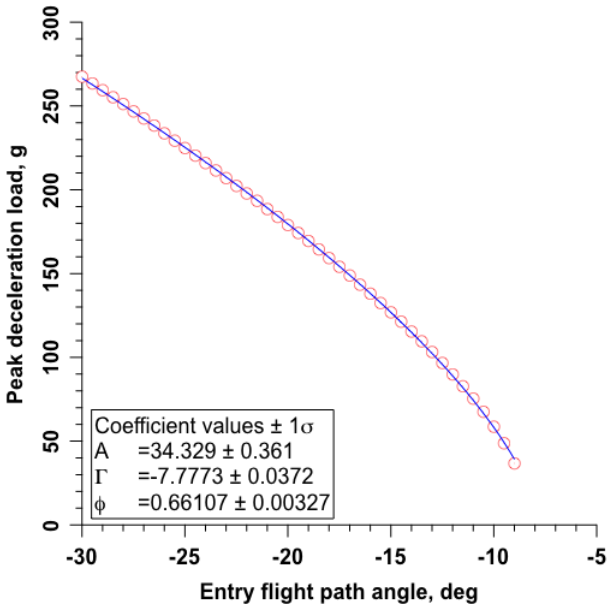

Figure 4. Variation with EFPA of peak deceleration load for m_E= 2000 kg and 11.6 km/s entry velocity. The open symbols are 3DoF predictions and the line is a curve fit of the form shown in Eq. 6.

Table 2. Coefficients of curves fit to peak deceleration loads for a 2000 kg entry mass capsule

		V_E, km/s								
		11.6	**11.2**	**10.8**	**11.6**	**11.2**	**10.8**	**11.6**	**11.2**	**10.8**
β_E, kg/m^2	D_b, m	$A(V_E,\beta_E)$			$\Gamma(V_E,\beta_E)$			$\phi(V_E,\beta_E)$		
388	**2.5**	33.6	28.5	28.8	–7.94	–7.49	–7.65	0.651	0.681	0.656
198	**3.5**	34.3	31.1	28.9	–7.78	–7.50	–7.35	0.661	0.669	0.668
120	**4.5**	34.7	31.4	30.7	–7.68	–7.41	–7.44	0.671	0.679	0.664

Nominal Cases: Mechanical constraint (peak pressure load)

We turn next to the other mechanical performance constraint – the pressure load.

Figure 5 shows the variation with EFPA of peak pressure loads for an entry mass of 2000 kg. Curves are shown for all three entry velocities and three entry ballistic coefficients – 120, 198, and 388 kg/m^2 (a factor of 3 spread between low and high). We observe the following:

(i) Peak pressure loads increase with increasing EFPA for *all* entry velocities and ballistic coefficients, which is as expected. However, there is a very strong dependence on ballistic coefficient – as the ballistic coefficient decreases, so does the peak pressure load. The trend, however, is opposite that of peak deceleration loads, which increase with *decreasing* ballistic coefficient (Fig. 3).

(ii) For a given EBC (curves of one family—solid, or dashed, or dash-dotted) the highest pressure loads correspond to the highest entry velocity (11.6 km/s). Between the highest and lowest entry velocities, the peak pressure loads at an EFPA of -30° differ by no more than 30%, which is a little larger than the 15% we saw in the case of peak deceleration loads.

(iii) For a given entry velocity (curves of one color – red, or green, or blue) the highest pressure loads correspond to the highest ballistic coefficient (388 kg/m^2). Between the highest and lowest ballistic coefficients, the maximum difference in pressure loads at an entry flight path angle of -30° is roughly a factor of 3, suggesting that this difference scales directly as ballistic coefficient.

(iv) At an entry angle of roughly -9.75°, the peak pressure loads are nearly independent of the entry velocity. However, there is still a dependence on ballistic coefficient. For the highest ballistic coefficient of 388 kg/m^2 (2.5 m diameter heatshield), the maximum pressure load at -9.75° EFPA is roughly 3.5 bar.

Since the highest pressure loads occur for the highest entry velocity of 11.6 km/s for all three ballistic coefficients, it is sufficient to work with curves corresponding to this entry

velocity to determine the steepest entry angles for a prescribed pressure load limit.

Dashed horizontal lines at 5 and 10 bar are also shown in Fig. 5. The intersections of these lines with the peak pressure load curves for the highest entry velocity (11.6 km/s) are shown as dashed vertical lines in the plot. The arrows indicate the direction in which the vertical lines move with decreasing peak pressure load limits to suggest that the pressure load limit too determines the steepest entry flight path angle for a given ballistic coefficient.

If peak pressure loads cannot exceed 10 bars, then the steepest EFPA is –16.75° for an EBC of 388 kg/m^2. For the lowest EBC of 120 kg/m^2, the steepest EFPA is outside our chosen EFPA interval and peak pressure load is not a constraint.

If peak pressure loads cannot exceed 5 bar, then the steepest EFPA is –10.75° for an EBC of 388 kg/m^2, and –23.5° for an EBC of 120 kg/m^2, which is a 12.75° interval in EFPA.

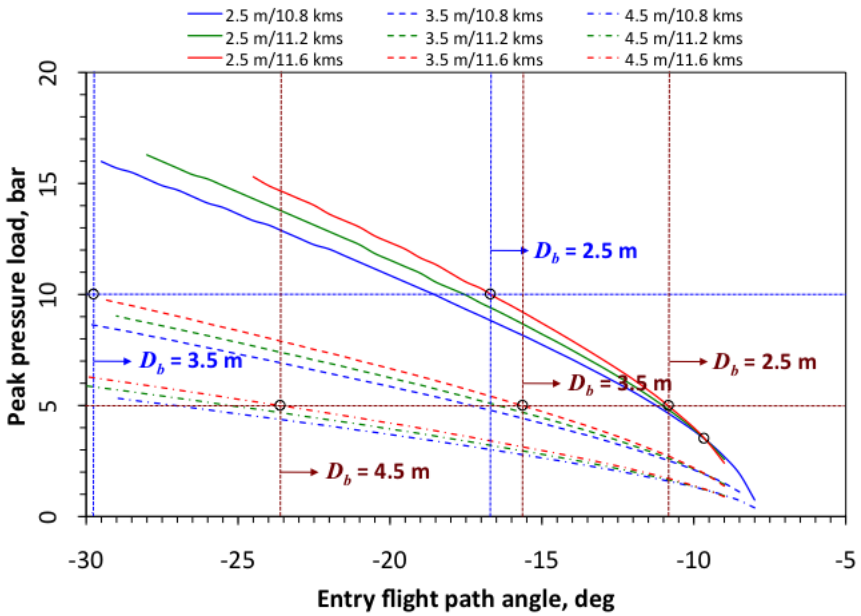

Figure 5. Variation with entry flight path angle of peak pressure load for m_E = 2000 kg (EBC = 120, 198, and 388 kg/m^2) and various entry velocities. Horizontal dashed lines are shown at 5 and 10 bar, and at the intersections of these lines with the peak pressure load curves, the corresponding entry flight path angles are shown as vertical dashed lines. At roughly –9.5° EFPA, the pressure load is nearly independent of entry velocity for each ballistic coefficient.

As with the deceleration loads, we can work with the alternative analytical method instead of the graphical one shown in Fig. 5.

We still retain the curve fit form shown in Eq. 6, but determine the new values of the coefficients for peak pressure loads. For a prescribed value of p_{Peak}, Eq. 6 is easily inverted to obtain the corresponding value of EFPA, γ_E. This provides a cross check against results of the graphical method.

Figure 6 shows a sample fit to peak pressure loads for a 3.5 m diameter capsule of 2000 kg entry mass and an entry velocity of 11.6 km/s. The values of A, Γ, and ϕ obtained by fitting the data are also shown in the figure.

Applying Eq. 6 to all peak pressure load curves (all nine of them) shown in Fig. 5 results in the entries shown in Table 3. The inflections in Γ and ϕ at 11.2 km/s are interesting, but cannot be explained easily without finer resolution in entry velocity. The dependence of the coefficients on EBC is somewhat weak. The lead coefficient A shows a very strong dependence on EBC.

Comparing the entries in Tables 2 and 3, we see that the coefficients Γ and ϕ are very similar for both peak deceleration and peak pressure loads, which is not very surprising. However, values of the lead coefficient A are different, which is as expected from the different scaling.

As with the peak deceleration load, the dependence of the curve-fit coefficients on either entry velocity or EBC could be pursued further. However, such an undertaking will require much finer resolution in both variables.

We now have two performance constraints, both of which provide limits on the steepest EFPA. The obvious questions are: (i) Can both these constraints be active at the same time? and (ii) Is there a critical ballistic coefficient at which both constraints return the same EFPA? The latter question is harder to answer because we have only sampled the ballistic coefficient variable at a finite number of points, *i.e.*,

ballistic coefficient is not a continuous variable in the present work. However, both questions can be answered by applying the graphical procedure (outlined in Figs. 3 and 5) to all 15 cases of in Table 1.

Table 3. Coefficients of curves fit to peak pressure loads for a 2000 kg entry mass capsule

		V_E, km/s								
		11.6	**11.2**	**10.8**	**11.6**	**11.2**	**10.8**	**11.6**	**11.2**	**10.8**
β_E, kg/m^2	D_b, m	$A(V_E,\beta_E)$			$\Gamma(V_E,\beta_E)$			$\phi(V_E,\beta_E)$		
388	**2.5**	2.47	2.09	2.11	-7.95	-7.50	-7.65	0.648	0.679	0.653
198	**3.5**	1.28	1.16	1.08	-7.77	-7.51	-7.34	0.661	0.669	0.668
120	**4.5**	0.78	0.71	0.69	-7.69	-7.42	-7.44	0.669	0.677	0.663

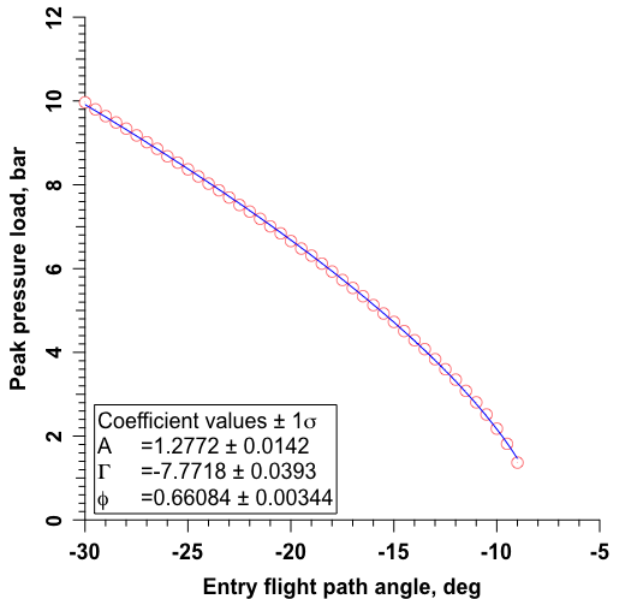

Figure 6. Variation with EFPA of peak pressure load for m_E= 2000 kg and 11.6 km/s entry velocity. The open symbols are 3DoF predictions and the line is a curve fit of the form shown in Eq. 6.

Deceleration Load Limit vs. Pressure Load Limit

We attempt to answer the question whether there is a "critical" ballistic coefficient at which *both* constraints are active, *i.e.*, have the same EFPA for prescribed values of peak deceleration and peak pressure load limits.

Pressure loads experience a very steep fall off with decreasing ballistic coefficient (Fig. 6). The trend strongly suggests that there is a "knee" in the critical pressure *vs.* ballistic coefficient curve, and an attempt is made to determine this "knee" using the bar chart shown in Fig. 7.

Each entry mass considered in the present work is a horizontal bar in Fig. 7, and the length of each bar spans the ballistic coefficient range covered by various diameters (ranging from 2.5 m to 4.5 m) of the heatshield. Shown on top of each bar are the diameters that correspond (approximately) to the ballistic coefficients in the present study. The bars are colored by the findings of analysis of trajectories generated as part of this study. Regions colored yellow indicate that the EFPA window is closed at the steep end by the deceleration load constraint, and regions colored green indicate that the EFPA window is closed by the pressure load constraint. The gray areas between indicate the ballistic coefficient range in which deceleration load ceases to be an active constraint and pressure load becomes the driver in closing the EFPA window at the steep end. The diameters for which the pressure load constraint is a definite driver are indicated in red in Fig. 7.

We see that the ballistic coefficient range at which the switch occurs lies between 250 and 260 kg/m^2. Therefore, there is a "critical" EBC at which the deceleration load and pressure load constraint yield the same interval closing entry flight path angle. Denoting this "critical" EBC as $\beta_{E,\text{crit}}$, we can determine the equivalent heatshield diameter, $D_{b,\text{crit}}$, from

$$D_{b,\text{crit}} = \sqrt{\frac{4m_E}{\pi C_D \beta_{E,\text{crit}}}} \tag{7}$$

This heatshield diameter is to be interpreted as the *smallest diameter* that can be flown *without* violating the peak pressure load constraint, which we have assumed to be 10 bar. Using 255 kg/m^2 as the value of $\beta_{E,\text{crit}}$ and an entry mass of 316.5 kg (mass of PVLP), we compute the minimum or "critical" diameter of the heatshield to be 1.227 m. Although further computations are necessary to get the precise value of the "critical" EBC, it is comforting to see that the present results are consistent with Pioneer Venus – the 316.5 kg entry capsule had a 1.42 m diameter heatshield.

It should be borne in mind that this "critical" EBC is for a 10 bar limit on the peak pressure load. If the peak pressure load limit is reduced, the value of $\beta_{E,\text{crit}}$ will change (reduce) as well (Fig. 5). Although a lower pressure load limit is moot in the context of entry-grade carbon phenolic, this finding might have implications for newer materials being developed as alternates to entry-grade carbon phenolic.

Having worked with the mechanical constraints (or limits), we turn next to the thermal performance constraint, *viz.* the total heat load.

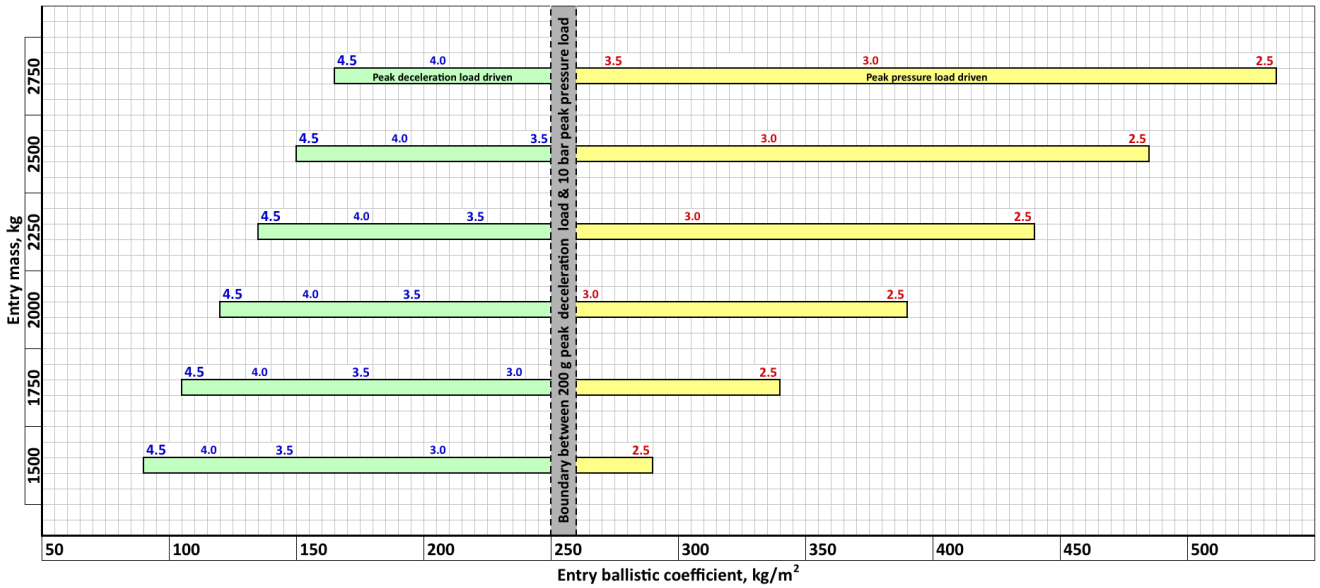

Figure 7. Bar chart of ballistic coefficient intervals in which the pressure load limit of 10 bar determines the closure of the entry flight path angle at the steep end of the interval. Also indicated on the bar chart are the diameters of the heatshields. Diameters for which the pressure limit determined EFPA interval closure are shown in red. The shaded region between EBC values of 250 and 260 kg/m^2 is where the peak deceleration and peak pressure loads switch roles in determining the steepest entry angle. These results are for a 200 g peak deceleration load and 10 bar peak pressure load mission profile.

Nominal Cases: Thermal constraint (total heat load)

The thermal performance constraint, which is primarily the total heat load, determines how shallow the EFPA can be.

Figure 8 shows the variation with EFPA of total heat load at the stagnation point for an entry mass of 2000 kg. Curves are shown for all three entry velocities and three entry ballistic coefficients. We observe the following:

(i) Total heat load is strongly dependent on ballistic coefficient *and* entry velocity.
(ii) For a given EBC (curves of one family—solid, or dashed, or dash-dotted) the highest total heat loads correspond to the highest entry velocity (11.6 km/s).
(iii) For a given entry velocity (curves of one color – red, or green, or blue) the highest total heat loads correspond to the highest ballistic coefficient (388 kg/m^2). Between highest and lowest ballistic coefficients, the peak heat fluxes differ by as much as a factor of 3.
(iv) In all cases, there is an upturn in total heat load at the shallow end of the EFPA interval.
(v) These results are consistent with the contours shown in Fig. 1.

As mentioned earlier, large total heat loads result in large thicknesses of the thermal protection material to keep the adhesive bondline at 250 °C. Deferring TPS mass fraction and material properties for now, we therefore seek "reasonable" heat loads that yield "reasonable" thicknesses of the thermal protection material, and the EFPAs corresponding to these heat loads. Since there is subjectivity in coming up with a "reasonable" total heat load limit, determination of the EFPA that closes the viable window at the shallow entry end becomes a contentious task. We have made an attempt here to develop a semi-rigorous metric to determine the EFPA window closure.

We know the total heat load (Q) rises sharply beyond a certain EFPA (Fig. 8). Therefore, we make an attempt to determine the "knee in the curve" (point of maximum curvature) of the Q-γ_E distributions. Instead of using a graphical method, or even a numerical approach with Eq. 4, to compute the curvature, $\kappa(\gamma_E)$, of the total heat load distributions, we use an analytical approach.

We first curve fit the total heat load distributions using a function of the form given in Eq. 6, and then evaluate curvature (Eq. 4) analytically.

Figure 9 shows a sample fit to total heat loads for a 3.5 m diameter capsule of 2000 kg entry mass and an entry velocity of 11.6 km/s. The values of A, Γ, and ϕ (curve-fit coefficients in Eq. 4) obtained by fitting the data are also shown in the figure.

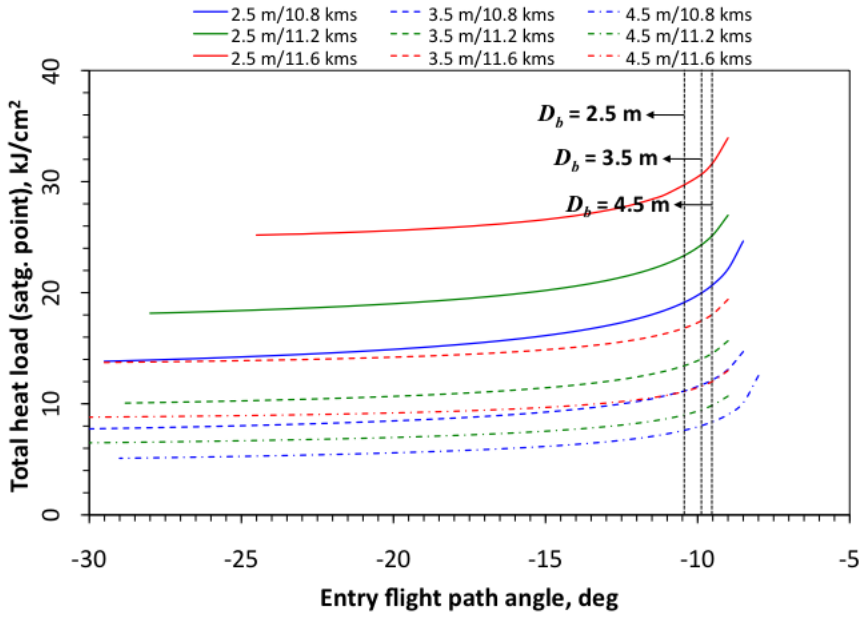

Figure 8. Variation with entry flight path angle of total heat load (at the stagnation point) for m_E = 2000 kg (EBC = 120, 198, and 388 kg/m^2) and various entry velocities. The vertical dashed lines represent EFPAs at which the total heat load distributions (for an entry velocity of 11.6 km/s) have maximum curvature.

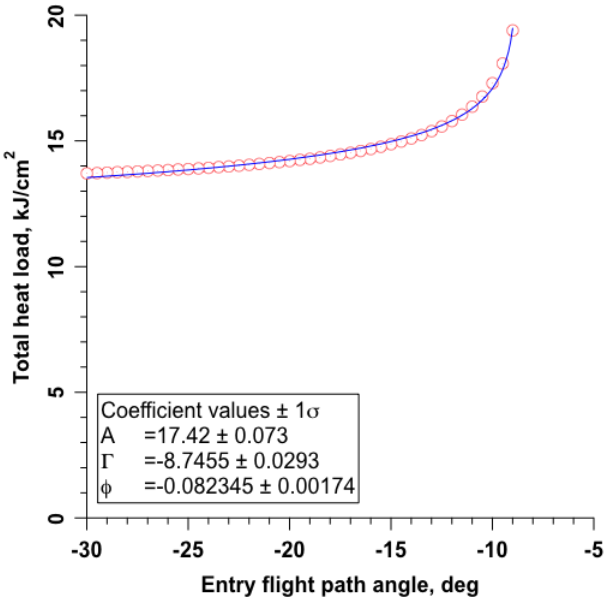

Figure 9. Variation with EFPA of total heat load for m_E =2000 kg and 11.6 km/s entry velocity. The open symbols are 3DoF predictions and the line is a curve fit of the form shown in Eq. 6.

Applying Eq. 6 to all total heat load curves shown in Fig. 8 results in the entries shown in Table 4.

Comparing the values of Γ (interpreted crudely as a skip out EFPA) in Table 4, with the corresponding values in Tables 2 and 3, we see a shift of almost 1° towards the steeper end of the EFPA interval. These results confirm what we expected – the "knee in the curve" (of the total heat load distributions) is away from the skip out boundary.

The distributions of curvature of total heat load, computed using Eq. 4 with the entries given in Table 4, are shown in Fig. 10. For each V_E-β_E combination, there is a distinct peak in curvature, and each peak is the "knee in the curve" of the corresponding total heat load distribution. The values of EFPA corresponding to the peaks in curvature (Fig. 10) are shown in Table 5. The peaks depend weakly on entry velocity, but shift by as much as 1.0° with a factor of 3 change in EBC.

Table 4. Coefficients of curves fit to total heat loads for a 2000 kg entry mass capsule

		V_E, km/s								
		11.6	**11.2**	**10.8**	**11.6**	**11.2**	**10.8**	**11.6**	**11.2**	**10.8**
β_E, kg/m^2	D_b, m	$A(V_E,\beta_E)$			$\Gamma(V_E,\beta_E)$			$\phi(V_E,\beta_E)$		
388	**2.5**	30.7	24.8	22.2	–8.75	–8.56	–7.93	–0.075	–0.108	–0.159
198	**3.5**	17.4	14.5	12.8	–8.75	–8.49	–8.06	–0.082	–0.123	–0.167
120	**4.5**	11.6	9.8	9.3	–8.71	–8.48	–7.78	–0.095	–0.138	–0.201

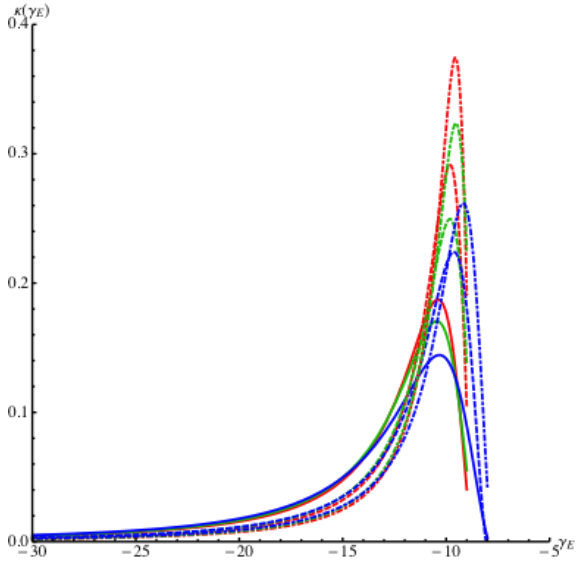

Figure 10. Variation with EFPA of curvature (Eq. 4) of total heat load distributions for m_E = 2000 kg and nine V_E-β_E combinations (10.8, 11.2, and 11.6 km/s and 2.5, 3.5, and 4.5 m diameter).

Table 5. EFPAs corresponding to peak curvature in heat load distributions for m_E = 2000 kg

		V_E, km/s		
		11.6	**11.2**	**10.8**
β_E, kg/m^2	D_b, m	γ_E at κ_{max} of Q		
388	**2.5**	–10.40	–10.45	–10.32
198	**3.5**	–9.81	–9.81	–9.62
120	**4.5**	–9.55	–9.52	–9.17

We could use the EFPA values in Table 5 to close the shallow end of the EFPA window, *i.e.*, prescribe these values as the shallowest one should enter the atmosphere of Venus. The vertical dashed lines in Fig. 8 represent these limits for an entry velocity of 11.6 km/s. Just because we have "closed" the EFPA window does not mean that we have established their viability. To do so would require that we have to consider both the heatshield mass fraction (Eq. 5) and peak heat flux. However, before we take up these ideas next, we emphasize that a material is *not* involved in the total heat load argument presented so far. The total heat load is simply a time-integrated heat flux, and the heat flux at the stagnation point (Eq. 2) is independent of the material. However, the heatshield mass fraction argument presented next *does* depend on the choice of material for the heatshield.

Nominal Cases: TPS mass fraction

Figure 11 shows the variation with EFPA of *unmargined* heatshield mass (based on uniform thickness of entry-grade carbon phenolic) for an entry mass of 2000 kg. Curves are shown for all three entry velocities and three entry ballistic coefficients. Several thin vertical dashed lines are shown in the figure. The blue vertical lines represent EFPA limits determined by either the 200 g limit on peak deceleration loads or by the 10 bar limit on peak pressure loads. Referring back to Fig. 5, we see that for the 2000 kg/2.5 m dia. heatshield (EBC of 388 kg/m^2), the steepest EFPA is determined by the 10 bar pressure limit; the peak deceleration load limit of 200 g determines the steepest EFPA for the other two diameters at this entry mass. The black vertical lines represent EFPA limits determined by the total heat load. The EFPA space between like pairs of vertical lines, indicated by double-headed green arrows, represents the first estimate of the viable EFPA window for each diameter (equivalently each EBC).

We now attempt to get a second estimate of the viable EFPA window by prescribing a "desired" heatshield mass, which is simply the product of a "desired" mass fraction (of the heatshield) and the entry mass (Eq. 5). We could use the Pioneer Venus probes for these fractions or rely on the estimates provided by the mission concepts [2-4]. The mass fraction of entry-grade carbon phenolic used in PVLP was 0.09, i.e., 9% of the entry mass (of 316.5 kg) was taken up by just the carbon phenolic material; this fraction was 0.13 for the three small probes (91 kg) of the Pioneer Venus mission. These mass fractions are from as-flown designs. However, the mass fractions for the concept missions [2-4] ranged from 0.17 to 0.22 (values back calculated using the thicknesses stated, wetted areas, and mass density of entry-grade carbon phenolic).

We see that there can be variability in mass fractions, perhaps due to variability in mission requirements, or perhaps due to different assumptions, or both. The best that can be done then is to determine the sensitivity of the EFPA window to an *assumed* fraction. However, we have to be cautious here because the estimates of heatshield mass that we have are *unmargined*. Since the present paper is not about heatshield design, and hence, we do not have a margins policy, we have simply used an arbitrary value of 0.1 of the unmargined heatshield mass fraction to illustrate a few key points.

The thin horizontal dashed line is shown in Fig. 11 for a heatshield mass of 200 kg for a 2000 kg entry mass, *i.e.*, for a mass fraction of 0.1. First, we notice that a 4.5 m diameter heatshield has *no* viable entry space based on this assumed mass fraction. Second, the shallow end of the EFPA window for the 3.5 m diameter heatshield closes at roughly -19°, which is close to the steep end limit of roughly –22°. Third, the first estimate of viable EFPA space for the 2.5 m dia. heatshield remains unchanged. Fourth, to enable the larger diameter heatshield will require an increase in the stipulated value of 0.1 for mass fraction.

There is little further to be gained from working with the mass fraction argument, especially since it requires both a margins policy *and* a clear mission requirement and/or mass allocation.

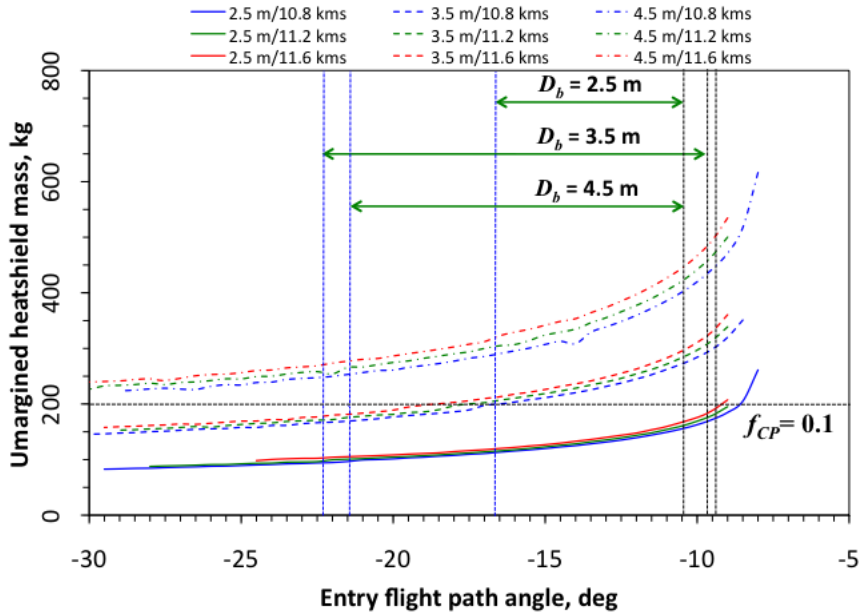

Figure 11. Variation with entry flight path angle of *unmargined* heatshield mass for m_E = 2000 kg (EBC = 120, 198, and 388 kg/m^2) and various entry velocities. The vertical lines represent EFPA limits derived from mechanical and thermal constraints. The thin horizontal dashed line at 200 kg represents a heatshield mass fraction of 0.1

Nominal Cases: Material heat flux limit

The chief remaining consideration is the heat flux performance of the material. Ablative materials usually have a threshold heat flux below which their performance is diminished, making them mass inefficient. This heat flux threshold is not available in the open literature. Therefore, we choose not to take it into consideration. The only thing one could do is to determine the heat flux values corresponding to the EFPA limits to see if these values exceed the performance requirements of the mission.

We conclude here by stating that only a sampling of the results of this study has been provided in the present paper. Complete details are available from a comprehensive document [28] currently in preparation.

6. Ground Test Considerations

One aspect not addressed in the present work is testing of materials (entry-grade carbon phenolic or other). Ground-based test facilities, such as arc jets, also have to be factored into the constraints because there are limits on the test heat fluxes and pressures they can provide. Depending on the trajectory, some of the predicted pressure-heat flux combinations could lie outside the operational envelopes of these ground-based facilities. Furthermore, some of the facilities developed at NASA Ames Research Center (ARC) during the Galileo program no longer exist.

Based on the results shown in Table 6, the predicted heat fluxes and pressures at the low end are roughly 2 kW/cm^2 and 5 bar. With an appropriate test article design, heat fluxes of this level can be achieved in the 60 MW Interaction Heating Facility (IHF) arc jet at NASA ARC. For instance, one could test small (10.16 cm diameter) sphere-cone geometries in the smallest nozzle (15.24 cm exit diameter) that is currently available in the IHF. However, stagnation point pressures greater than 1.5 bar cannot be achieved with this nozzle. To raise the pressure, the nozzle exit diameter will have to be smaller. Indeed, there is currently a plan at NASA ARC to develop a nozzle with an exit diameter of 7.62 cm (3 inches). While such a nozzle will be more able to provide the high heat fluxes and pressures necessary to test and qualify materials, modeling and test design (in terms of coupon size and thermal response including sidewall effects) will pose more of a challenge. A piecewise approach to testing and flight qualification, as discussed in the paper of Venkatapathy *et al*. [29], would probably be called for.

7. Summary

We have considered the legacy 45° sphere-cone aeroshell geometry for entries into Venus, which is called out as a priority destination in the latest NRC Planetary Science Decadal Survey. Guided by some of the mission studies performed in support of the latest Decadal Survey, we have considered a number of entry mass and diameter combinations and a range of entry velocities as initial conditions for atmospheric entry into Venus. Specifically, we have considered combinations of entry masses of 1500, 1750, 2000, 2250, and 2750 kg, diameters of 2.5, 3.5, and 4.5 m, and entry velocities of 10.8, 11.2, and 11.6 km/s.

Furthermore, we have limited the present study to ballistic entries that tie back to Pioneer Venus legacy.

With the knowledge of entry ballistic coefficient, entry velocity, and heading angle, we have rapidly generated hundreds of 3DoF trajectories using the in-house code, *TRAJ*. We have covered an EFPA range from near skip out at the shallow end to -30° at the steep end, with an increment of 0.5°. All trajectory computations are terminated at a Mach number of 0.8, assuming parachute deployment at this point. For each trajectory we have tracked the peak deceleration load (or g load), the peak pressure at the stagnation point (or p load), the peak total heat flux (both convective and radiative heat fluxes computed using correlations based on the nose radius and freestream density and flight speed), the total heat load, and the final altitude at Mach 0.8. Further, for each trajectory, using the *FIAT* option built into *TRAJ*, the *unmargined* thickness (at the stagnation point of the heatshield) of *entry-grade carbon phenolic* (for which a calibrated material thermal response model is readily available) has been computed. Assuming this thickness to be uniform, we have computed the mass of the heatshield. The trajectory and material sizing computations are calibrated against similar data for PVLP.

With this coverage of EFPA, we have imposed constraints based on mechanical and thermal performance of the heatshield material. For mechanical performance we have assumed a deceleration load limit of 200 g on the science payload and a pressure load limit of 10 bar on the heatshield material. Applying these constraints on the *TRAJ*-predicted deceleration and pressure loads, we have shown that they determine the steepest possible entries. Furthermore, we have shown that, for the chosen ballistic coefficients, the constraints on deceleration loads and pressure loads are not active at the same time. For most cases the operating constraint that determines the steepest possible entry is the deceleration load limit of 200 g. However, as the EBC increases, the 10 bar limit on pressure becomes increasingly important. Analysis of computed trajectories shows the existence of "critical" EBCs beyond which the steepest entry angle is determined by the pressure load and not the deceleration load. The thermal performance of the material determines the shallowest possible entries, and we have assumed a threshold based on inflections in total heat load distributions. Using the steep and shallow end limits on EFPA determined by mechanical performance and thermal performance constraints, respectively, we have determined the viable EFPA windows (if any) for the many mass and diameter combinations, thus meeting the primary objective of the present work. A key finding is that there is a critical ballistic coefficient beyond which the structural integrity of the material under pressure loads becomes limiting. For the above mechanical constraint choices, this $\beta_{E,crit}$ is about 250 kg/m^2.

We hope that apart from establishing viable entry corridors for Venus missions (all predicated on the use of entry-grade carbon phenolic on a legacy 45° sphere-cone geometry), the results of the present study will be useful in the development of a new class of ablators. Based on the analysis presented, we think that a key driver in the development of a new class of ablators for *rigid aeroshells* is the pressure load, and the higher the spallation pressure load limit of the new materials, the more the EFPA window for ballistic entries can be opened up.

We add that the methodology presented here initially employed a graphical approach to analysis of 3DoF results. However, we have also demonstrated that it is possible to use analytical methods to determine first estimates of viable EFPA intervals. Essentially this means that with a modest investment in the development of software tools, we can develop an analysis framework, which significantly reduces analysis time, allows for examination of larger and finer set of parameters, and generalizes to other planetary entries.

ACKNOWLEDGEMENTS

The Entry Systems and Technology Division at NASA Ames Research Center supported the authors, Dinesh Prabhu and Gary Allen, by Contract NNA10DE12C to ERC, Inc. The authors also acknowledge helpful discussions with Raj Venkatapathy, Bernie Laub, Joseph Garcia, Kathy McGuire, Loc Huynh, and John Karcz from Ames Research Center. Thorough reviews of the manuscript by David Saunders, Don Ellerby, Brandon Smith, Paul Wercinski, and Ethiraj Venkatapathy are deeply appreciated by the authors.

REFERENCES

[1] National Research Council, *Visions and Voyages for Planetary Science in the Decade 2013-2022*, National Academies Press, 2012.

[2] Baker, C. L., and Karpati, G., "Venus Mobile Explorer," a Mission Concept Study in support of the NRC Planetary Science Decadal Survey, December 2009.

[3] Adams, M. L., and Baker, C. L., "Venus Intrepid Tessera Lander," a Mission Concept Study in support of the NRC Planetary Science Decadal Survey, April 2010.

[4] Adams, M. L., and Balint, T., "Venus Climate Mission Study," a Mission Concept Study in support of the NRC Planetary Science Decadal Survey, June 2010.

[5] Spilker, T. R., "Saturn Atmospheric Entry Probe Trade Study," First part of a Mission Concept Study in support of the NRC Planetary Science Decadal Survey, September 2010.

[6] Spilker, T. R., "Saturn Atmospheric Entry Probe Mission Study," Second part of a Mission Concept Study in support of the NRC Planetary Science Decadal Survey, April 2010.

[7] Van den Berg, M., and Falkner, P., "Study Overview of the Venus Entry Probe: An ESA Technology Reference Study," ESTEC document SCI-AP/2006/173/ VEP/MvbB, Issue 2, Rev. 3, February 2007.

[8] Sengupta, A. and Hall, L., "Challenges of a Venus Entry Mission," 2011 IEEE Aerospace Conference, Big Sky, MT, 2012.

[9] Sengupta, A., Cruz, J., Prabhu, D., and Wercinski, P., "Development of a Venus Entry System for the Surface and Atmospheric Geochemical Explorer (SAGE)," 9th International Planetary Probe Workshop, Toulouse, France, June 2012.
[10] Venkatapathy, E., Allen, G., Prabhu, D., and White, T., "Going Beyond Rigid Aeroshells: Enabling Venus and Outer-Planet In-Situ Science Missions with Deployables," 8th International Planetary Probe Workshop, Portsmouth, VA, June 2011.
[11] Gasch, M., "Re-Entry Grade Carbon Phenolic for NASA Planetary Probes - Past History and Assessment of Current Availability," 60th JPM/9th MSS/7th LPS/6th SPS/Joint Subcommittee Meeting (ITAR Restricted), Colorado Spring, CO, Apr.-May 2013.
[12] Peterson, D. L., and Nicolet, W. E., "Heat Shielding for Venus Entry Probes," *J. Spacecraft and Rockets*, Vol. 36, No. 3, 1974, pp. 382-387.
[13] Chen, Y.-K., and Milos, F. S., "Ablation and Thermal Response Program for Spacecraft Heatshield Analysis," *J. Spacecraft and Rockets*, Vol. 11, No. 6, 1999, pp. 475-483.
[14] Garcia, J.A., McGuire, K.M., Bowles, J.V., and Huynh, L.C., "Venus Lifting Trajectory Studies of a Low L/D and Mid L/D Aeroshell," currently an internal report which is expected to be presented at the 10th Intl. Planetary Probe Workshop, San Jose, CA, April 2013.
[15] Kliore, A. J., Moroz, V. I., and Keating, G. M. (editors), "The Venus International Reference Atmosphere," *Advances in Space Research*, Vol. 5, No. 11, 1985, pp. 1–304, Pergamon Press, Oxford, 1986.
[16] Gary A. Allen, Jr., Michael J. Wright, and Peter Gage, "The Trajectory Program (Traj): Reference Manual and User's Guide," NASA/TM-2004-212847, 2005.
[17] Fay, J. A., and Riddell, F. R., "Theory of Stagnation Point Heat Transfer in Dissociated Air," Journal of Aeronautical Sciences, Vol. 25, No. 2, 1958, pp. 73-85.
[18] Tauber, M. E., *Private communication*, October 2008.
[19] Wakefield, R. M., and Pitts, W. C., "Analysis of the Heat-Shield Experiment on the Pioneer-Venus Entry Probes," AIAA Paper 80-1494, July 1980.
[20] Anon., *Pioneer Venus Large and Small Probe Data Book*, HS507-5164, Hughes Aircraft Company, Los Angeles, California, 1976.
[21] Talley, R. L., *Pioneer Venus Deceleration Module – Final Report*, Re-entry and Environmental Systems Division, General Electric, Philadelphia, PA, 1978.
[22] Momentive, 180 East Broad Street, Columbus, OH 43215. http://www.momentive.com/Products/ShowTechnicalDataSheet.aspx?id=10319
[23] Dutta, S., Smith, B., Prabhu, D., and Venkatapathy, E., "Mission Sizing and Trade Studies for Low Ballistic Coefficient Entry Systems to Venus," 2012 IEEE Aerospace Conference, Big Sky, MT, March, 2012.
[24] Wright, M.W., White, T., and Mangini, N., "Data Parallel Line Relaxation (DPLR) Code User Manual Acadia – Version 4.01.1," NASA/TM-2009-215388, October 2009.
[25] Whiting, E. E., Park, C., Liu, Y., Arnold, J. O., and Paterson, J. A., "NEQAIR96, Nonequilibrium and Equilibrium Radiative Transport and Spectra Program: User's Manual," NASA RP-1389, NASA, December 1996.
[26] Ames Research Center, "Planetary Mission Entry Vehicles: Quick Reference Guide, v3," NASA/SP-2006-2041, 2006.
[27] Bienstock, B, "Pioneer Venus and Galileo Entry Probe Heritage," International Workshop on Planetary Probe Atmospheric Entry and Descent Trajectory Analysis and Science, Lisbon, Portugal, Oct. 2003.
[28] Prabhu, D. K., Allen, G. A., Jr., Cappuccio, G., Spilker, T. R., Hwang, H. H., and Moses, R. W., "Atmospheric Entry Studies for Saturn and Venus Missions: 45° Sphere-Cone Rigid Aeroshells and Ballistic Entries," NASA TM (in preparation), 2012.
[29] Venkatapathy, E., Laub, B., Hartmann, G. J., Arnold, J. O., Wright, M. W., Allen, G. A, "Selection and Certification of TPS: Constraints and Considerations for Venus Missions," 6th International Planetary Probe Workshop, Atlanta, GA, June 2008.

BIOGRAPHIES

Dinesh K. Prabhu *is a Senior Staff Scientist with ERC, Inc., an onsite contractor at NASA Ames Research Center. He received his B.Tech. in Aeronautical Engineering from the Indian Institute of Technology at Madras, India, and his Ph.D. in Aerospace Engineering from the Iowa State University at Ames, Iowa. His interests are in modeling and simulation of high-temperature hypersonic flow fields (for ground testing and flight), and in aerothermodynamic design of ground tests and atmospheric entry vehicles.*

Gary A. Allen, Jr. *is a Senior Research Scientist with ERC, Inc., an onsite contractor at NASA Ames Research Center. He received his B.S. in Engineering Physics from the University of California, Berkeley, and his Ph.D. in Aerospace Engineering from Stanford University, California. His main professional focus is modeling and simulation of spacecraft atmospheric entry through engineering approximations. He is the author of* TRAJ.

Gelsomina Cappuccio *is a Project Manager at NASA Ames Research Center. She received her BS in Mechanical Engineering from the University of Massachusetts at Amherst, MA, and her MS in Mechanical Engineering from the Pennsylvannia State University at*

State College, PA. Her interests are in the management of the application of newly developed technologies and scientific discoveries as it is applied to air breathing and entry vehicles. She was formerly the Project Manager of SOFIA Science, MSL Rover Sample Cache System, and X-37 Wing Leading Edge TPS.

Thomas R. Spilker *received his Ph.D. from Stanford University and spent the next 22 years at JPL, first as an NRC Postdoctoral Fellow for two years, then for two years in JPL's Science Division. From there he moved to space flight mission architecture in JPL's Division 31, where he bridged the gulf between science and engineering from 1995 until his retirement in mid-2012. He now operates his consulting business, Solar System Science and Exploration, in Monrovia, CA.*

Helen H. Hwang *is the Science Missions Development Manager in the Entry Systems and Technology Division at NASA Ames Research Center. She received her B.S., M.S., and Ph.D. in Electrical Engineering from the University of Illinois at Urbana-Champaign. She has participated in numerous planetary probe mission concept developments and proposals. Previously, she was the Thermal Protection System Project Manager for the Mars Science Laboratory mission.*

Robert W. Moses *is a Senior Researcher at NASA Langley Research Center in the Atmospheric Flight and Entry Systems Branch within the Engineering Directorate. He received his B.S. in Civil Engineering from North Carolina State University, his M.S. in Systems Engineering from Virginia Polytechnic Institute and State College, his M.S. in Mechanical Engineering from Stanford University, and his Ph.D. in Aeronautics & Astronautics from Stanford University. With other Centers, agencies, and industry, he has participated in flight projects in aeronautics and space mission directorates.*